Proceedings of the 21st ICSMGE, Vienna, Austria, 14 – 19 June 2026. Pistrol, Adam & Schweiger (eds.)
Published by: ÖGG, Austrian Society for Geomechanics, Salzburg, Austria, ISBN 978-3-9503898-4-5
https://doi.org/10.53243/ICSMGE2026-1331

Numerical modelling of a box-type foundation with control piles, pile number effect

Rubén Domínguez-Alfaro, Gabriel Auvinet, Norma Patricia López-Acosta
Instituto de Ingeniería, Universidad Nacional Autónoma de México, UNAM, México, rdomingueza@iingen.unam.mx

Rigoberto Rivera, Walter Paniagua, Marco Pérez, Rodrigo Rodríguez
Facultad de Ingeniería, Universidad Nacional Autónoma de México, UNAM, México

ABSTRACT: The purpose of this paper is to assess the static long-term behavior of a control pile foundation using three-dimensional finite element numerical models, depending of the number of control piles. The study allows identifying the influence of the number of piles on the long-term behavior of the foundation. This paper presents the first known case of numerical analysis of a group of control piles. The unconventional operation of this special type of foundation justifies the use of numerical models. Mexico City subsoil is characterized by thick layers of very soft clay (high compressibility and low shear strength) submitted to a consolidation process. Control piles are a special type of foundation used to reduce the apparent protruding, which may result from the interaction between deep foundations and the regional subsidence of Mexico City. Slab-piles load transmission is carried out through control devices placed on pile heads. Every control device is composed of a deformable cell and a steel load-bearing frame. In the long-term, pile heads and the slab exhibit different vertical displacements because these are not directly connected. This displacement difference causes the progressive crushing of the deformable cells. Due to such behavior, control piles require maintenance that involves unloading the pile, replacing the crushed cell with a new one and applying preload with a hydraulic jack. The results of numerical analyses show that the control pile number modifies behavior of the group, including the magnitude of apparent protruding and the distribution of the deformable cells requiring maintenance. At the end of the paper, comments and recommendations regarding the implemented methodology for carrying out analyses of this type of special foundation are provided.

KEYWORDS: Control pile, regional subsidence, finite element method, soft soils, negative skin friction, deep foundation.

1 INTRODUCTION

The Valley of Mexico is a closed basin where, in pre-Hispanic times, there were five large lakes. Currently, most of the lakes are dry due to various hydraulic projects that were built since colonial times. Mexico City is divided into three geotechnical zones, the hill zone, the transition zone and the lacustrine zone. The lacustrine zone is characterized by very soft clay deposits, 20 m to 50 m thick, with low shear strength and high compressibility (Auvinet *et al.*, 2017). The geotechnical environment of the Valley of Mexico also includes seismicity and regional subsidence.

The regional subsidence of Mexico City lacustrine zone is mainly due to the pore water pressure drawdown caused by deep pumping, which began in the 19th century to supply water to the population. Carrillo (1948) established the relationship between regional subsidence and the decrease in pore water pressure through the theory of consolidation. Since then, regional subsidence has continued and is still being studied.

As a result of the interaction with regional subsidence, many deep foundations present apparent protruding (Figure 1). Some of the consequences are a) cracking of adjacent structures due to differential settlement, b) loss of slab-soil contact, and c) loss of pile head confinement.

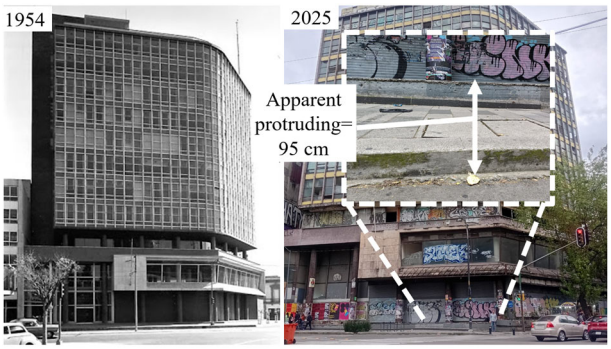

Figure 1. Apparent protruding of a foundation with friction piles.

Special foundations such as friction piles, negative friction piles, penetrating toe piles and interlocking piles have been used to reduce apparent protruding (Auvinet, 2018). In addition, González (1948) proposed the first known version of the control pile, characterized by a control device in the head of the pile.

2 CONTROL PILES

There are currently several versions of the control pile, which are modifications of the second version of González (1960). Basically, the control pile (Figure 2) is a pile whose head is structurally disconnected from the bottom slab of a box-type foundation. Slab-pile load transmission is carried out through a control device that consists of a deformable cell and a load-bearing frame.

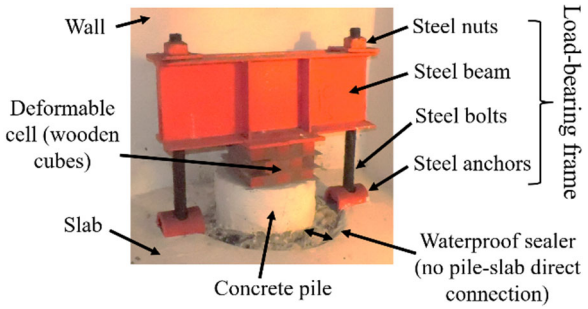

Figure 2. Basic arrangement of the control pile.

2.1 *Aims*

A control pile foundation is intended to control axial loads at pile heads and slab vertical displacements, both upward and downward. This allows the behavior of the foundation to be controlled.

2.2 *Uses*

Control piles have been implemented in over 600 buildings that have exhibited adequate behavior. Control piles are primarily used as an underpinning solution. Point-bearing or friction piles foundation can be converted to control piles (Auvinet & Gutiérrez, 1990) , for friction piles behavior is not documented. Control piles can also be implemented for new foundations.

2.3 *Main components*

Piles can be monolithic and driven using conventional procedures. *Mega* piles, which are prefabricated into 90 cm segments, are used primarily for underpinning in projects where space is limited. *Mega* piles are reinforced using corrugated rods or post tensioning cables.

The deformable cell is formed by a set of *caobilla* wooden cubes of 5 cm on each side arranged in three levels separated by steel plates. This type of cell is expected to present an elastoplastic behavior (González, 1960) and to transmit a constant load in a large deformation range. Other types of cells have also been used, such as polymer cylinders, neoprene plates, and steel hydraulic cells (López-Acosta & Martinez, 2021).

González (1960) proposed a load-bearing frame consisting of a pair of steel bolts, one end of which is embedded in the slab and the other is fixed with a nut, and a steel beam consisting of two type C steel sections. Other versions are available with more steel beams and bolts, as well as different types of stabilizers and anchors.

2.4 *Functioning and maintenance*

Control piles can be used to mitigate apparent protruding. In the long-term, the apparent penetration of the piles causes the deformable cells to crush. Maintenance is carried out when the deformable cells reach 30% vertical strain, as is common practice. Maintenance (Figure 3) consists of unloading the pile, replacing the crushed cell with a new one, and then preloading the pile with a hydraulic jack. Maintenance also includes trimming the excess length of the pile head.

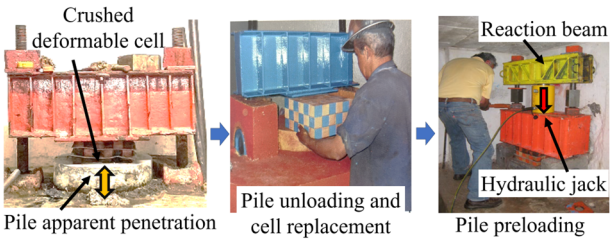

Figure 3. Main maintenance sequence.

The apparent penetration of the piles is due to the difference in vertical displacements between the piles and the slab that are not structurally connected (Figure 4). In the long-term, the pore water pressure drawdown causes consolidation of the clay layers. If the pore water pressure drawdown occurs in clay (upper soft clay) between the pile tips and the slab, the slab presents a greater vertical displacement than the piles.

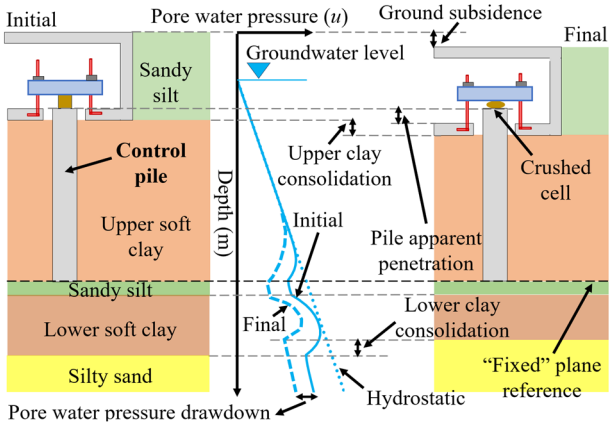

Figure 4. Long-term behavior of a control pile.

To ensure that the foundation follows the regional subsidence (reduction of apparent protruding), it is necessary to guarantee the continuous maintenance of the control piles and, if necessary, to modify their behavior. The behavior of the foundation is manipulated by control devices. If the nuts of the load-bearing frame are loosened, the reaction system is lost, causing free penetration of the pile and facilitating the gradual downward movement of the foundation and correction of any tilting of the building.

2.5 *Current analyses and design methods*

Currently there are four analytical methods to evaluate the failure limit state for control piles (Zeevaert, 1983, Tamez, 1990, PICOSA, 2014, Domínguez-Alfaro, 2024). Design of control piles is usually carried out based on empirical criteria. Prior to Domínguez-Alfaro (2024), no geotechnical-numerical analysis of control piles was published.

3 GEOTECHNICAL CONDITIONS OF THE SITE

Details of the calibration of the numerical model representing the regional subsidence of this site can be found in Domínguez-Alfaro (2024) and Domínguez-Alfaro *et al*. (2026). Based on field exploration carried out in two different years, the geotechnical model was able to reproduce the 128 cm free-field settlement that occurred during a period of 15 years.

3.1 *Stratigraphy*

The site is located in the lacustrine geotechnical zone. The stratigraphic profile of the studied site (Figure 5), characterized by thick lacustrine clay layers, is as follows:

1. Gravel and silty sand fill (RLL) with thickness of 3.0 m.
2. Sandy silt layer of firm consistency (CS), known as the "superficial crust", with thickness of 2.8 m.
3. Lacustrine clay of very soft consistency (FAS), with a water content between 200 and 500 %, as well as permeable lens intercalations (LP), thickness of 28.5 m.
4. Sandy silt of firm consistency (CD), known as the "first hard layer", with thickness of 2.1 m.
5. Lacustrine clay of medium consistency, with water content between 150 and 250 % and permeable lens intercalations (FAI). This layer presents a thickness of 4.1 m.
6. Silty sand and gravel layer very compact (DP), known as the "deep deposits", with thickness of 4.5m.

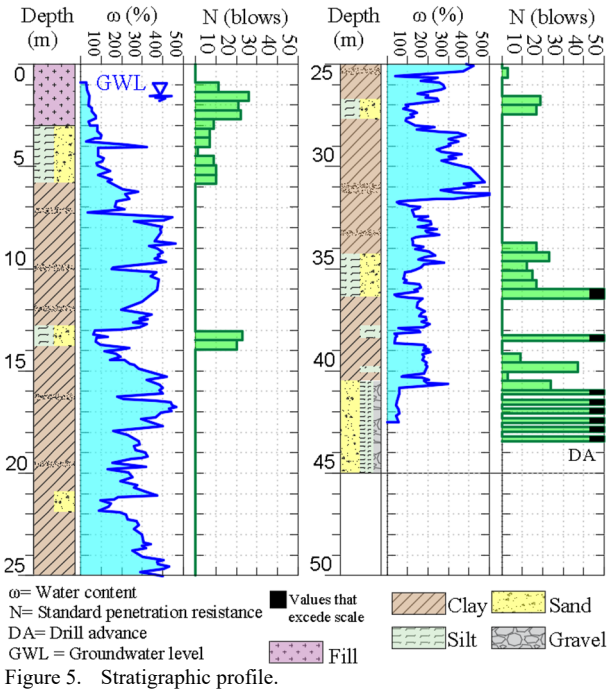

Figure 5. Stratigraphic profile.

3.2 *Geotechnical model*

Table 1 shows the geotechnical model of the site. The Hardening Soil (HS) and Soft Soil (SS) constitutive models were selected to represent the mechanical behavior of soils. Carrillo (1948) and Marsal (1969) demonstrated that regional subsidence analysis is associated with consolidation degrees less than 50%. Therefore, creep deformation with Mesri's C_α is considered to have a minimal influence. Drained mechanical parameters and undrained initial conditions are considered. The RLL, CS, LP 1 to LP 3, CD and DP are represented with the HS model. FAS 1 to FAS 7, FAI 1 and FAI 2 are analyzed with the SS model.

Table 1. Site geotechnical model.

Layer	Depth (m)	γ (kN/m^3)	e_0	c' (kPa)	φ' (°)	C_c
RLL	0.0 to 3.0	17.0	-	0	30	-
CS	3.0 to 5.8	15.0	2.2	35	40	-
FAS1	5.8 to 7.3	12.1	6.4	0	35	5.05
FAS2	7.3 to 12.8	11.3	8.1	0	35	7.95
LP1	12.8 to 13.8	17.0	1.5	40	40	-
FAS3	13.8 to 17.7	11.3	9.7	0	35	5.84
FAS4	17.7 to 20.9	12.0	6.5	0	35	4.65
LP2	20.9 to 21.9	15.5	2.2	20	25	-
FAS5	21.9 to 26.7	12.0	7.8	0	35	7.57
LP3	26.7 to 27.7	14.3	2.0	32	35	-
FAS6	27.7 to 31.5	12.2	7.0	0	35	6.74
FAS7	31.5 to 34.3	12.1	4.0	0	35	2.05
CD	34.3 to 36.4	16.0	1.7	55	40	-
FAI1	36.4 to 38.1	12.6	4.7	0	35	3.87
FAI2	38.1 to 40.5	11.2	4.9	0	35	4.38
DP	40.5 to 45.0	18.5	0.9	55	42	-

Table 1 Site geotechnical model (continued)

Layer	C_r	E_{50}^{ref} (MPa)	E_{oed}^{ref} (MPa)	E_{ur}^{ref} (MPa)	ν'_{ur}	k (cm/s)
RLL	-	10.0	8.0	80.0	0.2	2.1×10^{-3}
CS	-	7.0	5.6	56.0	0.2	2.6×10^{-7}
FAS1	0.45	-	-	-	0.2	2.7×10^{-8}
FAS2	0.57	-	-	-	0.2	1.0×10^{-8}
LP	-	18.8	15.0	60.0	0.2	1.5×10^{-6}
FAS3	0.55	-	-	-	0.2	1.7×10^{-8}
FAS4	0.33	-	-	-	0.2	1.6×10^{-8}
LP2	-	12.5	10.0	30.0	0.2	4.3×10^{-7}
FAS5	0.29	-	-	-	0.2	1.7×10^{-8}
LP3	-	16.0	12.8	38.4	0.2	4.7×10^{-6}
FAS6	0.22	-	-	-	0.2	1.9×10^{-8}
FAS7	0.15	-	-	-	0.2	6.5×10^{-9}
CD	-	35.0	28.0	112	0.2	1.4×10^{-7}
FAI1	0.15	-	-	-	0.2	1.6×10^{-8}
FAI2	0.15	-	-	-	0.2	7.1×10^{-9}
DP	-	40.0	32.0	96.0	0.2	1.4×10^{-7}

γ = natural volumetric weight, e_0= initial void ratio, c'= drained cohesion, φ' = drained internal friction angle, C_c= compression index, C_r= recompression index, E_{50}^{ref}= reference secant stiffness from drained triaxial test, E_{oed}^{ref}= reference tangent stiffness for oedometer primary loading, E_{ur}^{ref}= reference unloading/reloading stiffness, ν'_{ur} = unloading/reloading Poisson's ratio, k= permeability.

3.3 *Stress state*

Figure 6 (left) illustrates the evolution of the pore water pressure (u) profile that occurred during regional subsidence over a period of 15 years. This profile was calculated numerically and calibrated using on-site measurements. As the total vertical stress remained practically unchanged, the pore water pressure drawdown caused a gradual increase in the vertical effective stress (σ'_v), as illustrated in Figure 6 (right).

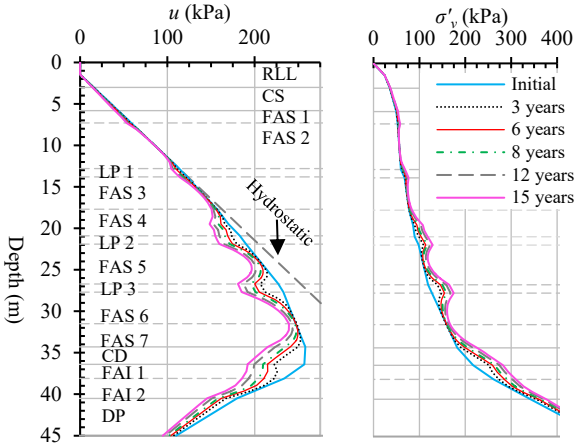

Figure 6. Stress profiles for different years of analysis.

4 NUMERICAL ANALYSIS OF THE BOX-TYPE FOUNDATION WITH CONTROL PILES

The aim is to determine the influence of the number of control piles on the static long-term behavior of a new foundation. The number of control piles (expressed as *S/D* ratio, where *D* is pile diameter, and *S* is center-to-center separation) is set as the research variable for the parametric numerical analysis. The numerical analysis is performed by means of 3D finite element numerical models with *Plaxis*® 3D software. Only one type of box-type foundation, uniform pressure on slab, pile, deformable cell and load-bearing frame are selected.

4.1 *Control pile foundation characteristics*

4.1.1 *Box-type foundation*

It is a square box-type foundation with a side of 24 m and a depth of 3 m. The structure exerts a uniform pressure of 80 kPa on the slab. The slab and wall thickness are 70 cm and 100 cm respectively. In addition, the slab presents 80 cm diameter holes to facilitate apparent penetration of the piles.

4.1.2 *Pile*

The monolithic concrete pile has a diameter (D) of 50 cm and a length of 31.3 m. The pile tip rests on the first hard layer (CD), at a depth of 34.3 m.

4.1.3 *Deformable cell*

The deformable cell has 3 levels of wooden cubes, separated by steel plates, and a 4 x 4 cubes arrangement at the base. The deformable cell measures 20 cm per side and 15 cm in height. Currently, *Plaxis* does not have a specific constitutive model to represent wood behavior; therefore, the HS model was selected as a practical approximation. The mechanical parameters of the deformable cell (Table 2) are obtained by calibrating numerical results with experimental measurements of compression tests (Figure 7) (López-Acosta & Martinez, 2021). The *Plaxis's* soil-test was used to analyze unconfined compression tests.

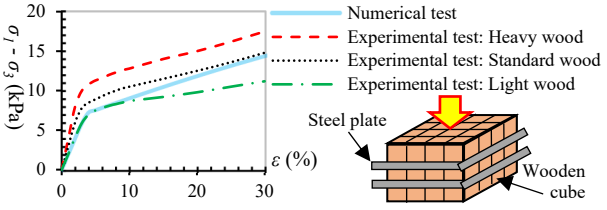

Figure 7. Calibration of the cell mechanical behavior: 4 x 4 cubes.

4.1.4 *Load-bearing frame*

The steel beam is 85 cm long, 37 cm wide and 38 cm high. The bolts, embedded in the slab, measure 5 cm in diameter. Both the beam and the bolts are made of structural steel grade A-36.

4.1.5 *Maintenance*

The control pile is maintained once the deformable cell has reached a vertical strain of 25%. In this case, the trimming of the pile head is omitted.

4.1.6 *Control pile group configuration and model geometry*

Four groups of uniformly distributed control piles are selected (Figure 8). The two symmetrical axes of the foundation are used to optimize the calculation time. Control pile groups are *S/D*= 12 (4 piles), *S/D*=8 (9 piles), *S/D*=6 (16 piles) and *S/D*=4.8 (25 piles). Three types of piles are classified: P1 are interior piles, P2 are piles at the slab edges, and P3 are corner piles.

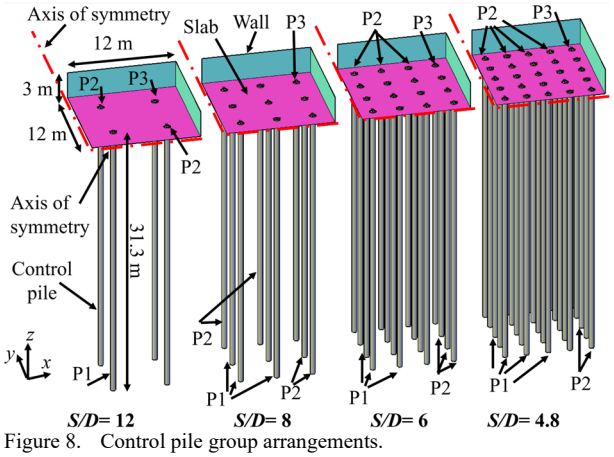

Figure 8. Control pile group arrangements.

4.2 *Model geometry and structural elements*

Figure 9 shows the geometry model for the *S/D*=12 group. The size of the finite elements decreases from the boundaries towards the center of the foundation, where the control devices have the smallest elements. The other three numerical models have the same geometry, except for the number of control piles.

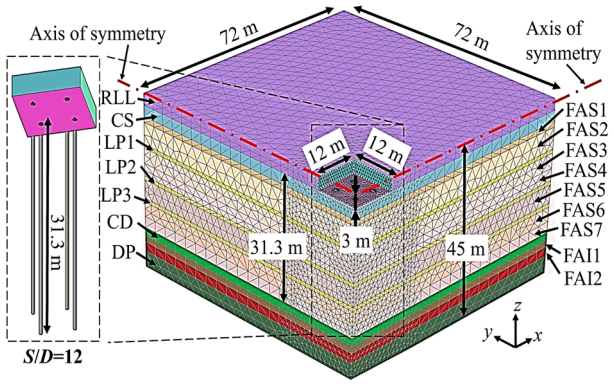

Figure 9. Geometry of numerical model for *S/D*=12 group.

Figure 10 shows the combination of structural elements used to represent the foundation. Tables 2 and 3 show the parameters of each structural element. Deformable cells are represented by the HS model, Mohr-Coulomb shear strength was assumed at interfaces while all other elements are considered elastic.

Table 2. Structural elements properties: C.

	γ (kN/m^3)	c' MPa	φ' (°)	E_{50}^{ref} (MPa)	E_{oed}^{ref} (MPa)	E_{ur}^{ref} (MPa)	ν'_{ur}
C	5.5	9	20	90	35	200	0.2

Table 3. Structural elements properties: P, I, B, T, L, W.

	γ (kN/m^3)	E (GPa)	ν	t (cm)	D (cm)	R_{int}
P	24	26	0.15	-	-	-
I	-	-	-	-	-	0.6
B	-	200	0.15	38	-	-
T	-	200	0.15	-	5	-
L	-	26	0.15	70	-	-
W	-	26	0.15	100	-	

E = Young modulus, ν= Poisson's ratio, t= thickness, D = diameter, R_{int}= ratio of the maximum shear stress at the interface with respect to the adjacent soil. The other literals were previously defined.

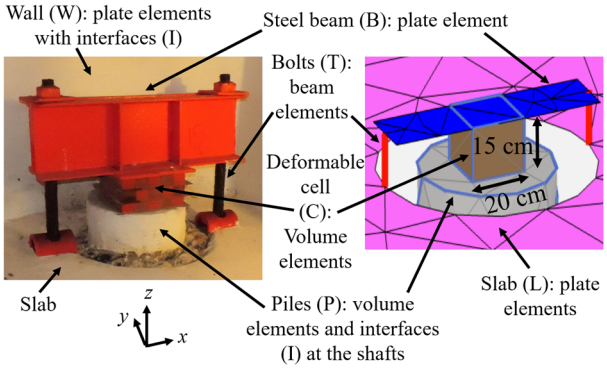

Figure 10. Numerical representation of the control pile foundation.

4.3 *Calculation steps*

Each numerical model has the following sequence:

1. Free-field. Stress state is as shown in Figure 6: initial state.
2. Control pile foundation construction (short-term).
3. Interaction of the control pile foundation with regional subsidence. Analysis time (years) is when any deformable cell reaches 25% of the vertical strain. The boundary condition is the stress state corresponding to that year.
4. Maintenance of the control pile group. Maintenance is performed on a single control pile at a time: pile unloading, crushed cell replacement and pile preloading (Figure 3).
5. Steps 3 and 4 are repeated one after another.

5 RESULTS

5.1 *Maintenance*

Table 4 summarizes the maintenance sequence (M) and the number of control piles intervened in each of them (N_P). *S/D*=12 and 8 groups tend to exhibit all control piles intervened in the same year. *S/D*=4.8 group requires its first maintenance after 15 years, but only for the P3 corner pile.

Table 4. Summary of maintenance of control piles.

Time	*S/D* = 12		*S/D* = 8		*S/D* = 6		*S/D* = 4.8	
(years)	M	N_P	M	N_P	M	N_P	M	N_P
3	1st	4	-	-	-	-	-	-
6	-	-	1st	9	-	-	-	-
8	2nd	4	-	-	-	-	-	-
12	3th	4	2nd	9	1st	3	-	-
15	4th	4	-	-	1st	5	1st	1

5.2 *Cell crushing*

Figure 11 shows a comparison between the deformed meshes, which are displayed at the year of the first maintenance of each pile group. Views correspond to close-ups of the control piles located on the center-corner diagonal. *S/D*=12 and 8 groups tend to exhibit uniform cell crushing and allow the maintenance of each pile in the group to be performed in the same year.

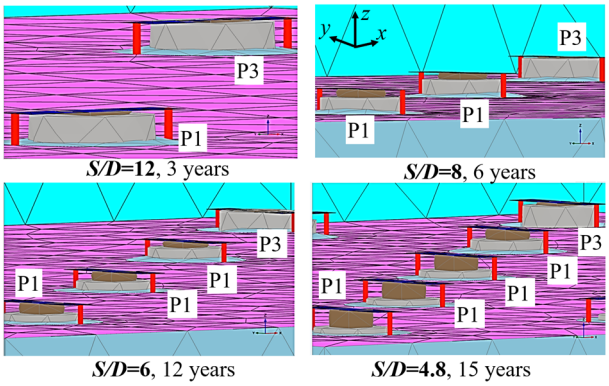

Figure 11. Deformed mesh amplified 3.3 times the natural scale.

5.3 *Apparent protruding*

Figure 12 shows the deformed meshes, amplified five times the natural scale, which are displayed for analysis of 15 years. Points A and B are references points used to compare between the apparent protruding magnitudes. Table 5 summarizes apparent protruding calculated for the same years shown in Table 4. The lowest apparent protruding magnitude is clearly observed in the case of the *S/D*=12 group.

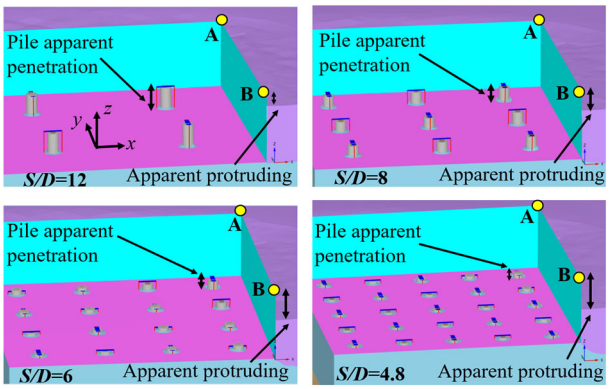

Figure 12. Deformed mesh amplified five times the natural scale, after 15 years.

Table 5. Summary of apparent protruding magnitude.

Time (years)	*S/D* = 12		*S/D* = 8		*S/D* = 6		*S/D* = 4.8	
	Apparent protruding magnitude (cm)							
	A	B	A	B	A	B	A	B
3	0.5	0.0	2.1	0.7	3.1	1.4	3.7	1.9
6	2.6	0.5	6.9	3.6	9.0	5.0	9.9	5.7
8	5.0	1.6	8.9	4.3	13	7.8	14	8.7
12	9.5	4.0	17	9.6	22	15	24	17
15	16	8.4	25	16	32	23	37	28

5.4 *Negative skin friction*

Figure 13 shows the vertical relative displacements (δ_{zR}) fields in the walls and piles after three and six years. The scale has been selected to clearly identify neutral planes (Reséndiz and Auvinet, 1973). In the *S/D*=12 and 8 groups the level of the neutral planes tends to be uniform, whereas, in the *S/D*=4.8 group the deepest level of the neutral plane occurs in the P3 corner pile. It is also observed that the negative skin friction in the walls starts at the corner and propagates towards the edges.

Other significant results are obtained by comparing the results of the extreme groups: *S/D*=12 and 4.8. Figure 14 shows vertical relative displacements fields in the piles after 15 years. The scale has been set to show only the displacements of the soil relative to the pile (negative skin friction). *S/D*=12 group presents a uniform distribution of negative skin friction with a magnitude larger than the *S/D*=4.8 group. *S/D*=4.8 group presents the greatest development of negative skin friction in the P3 pile.

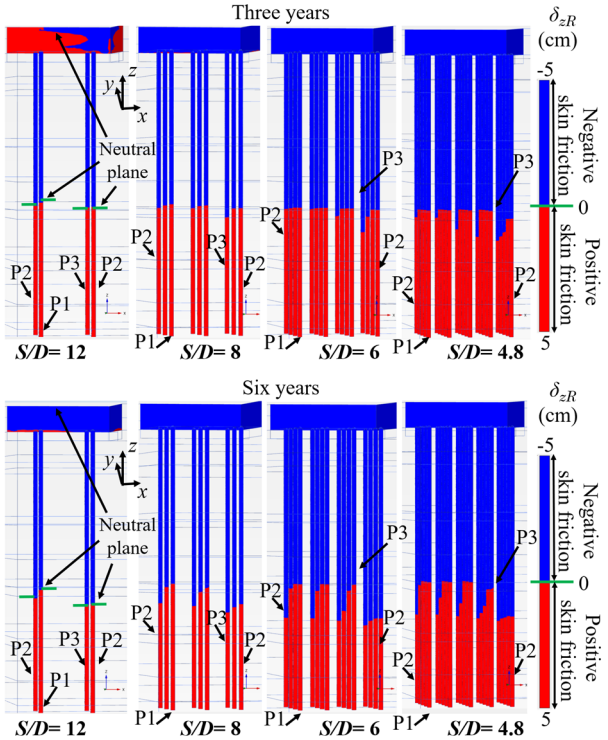

Figure 13. Vertical relative displacement fields, piles and walls.

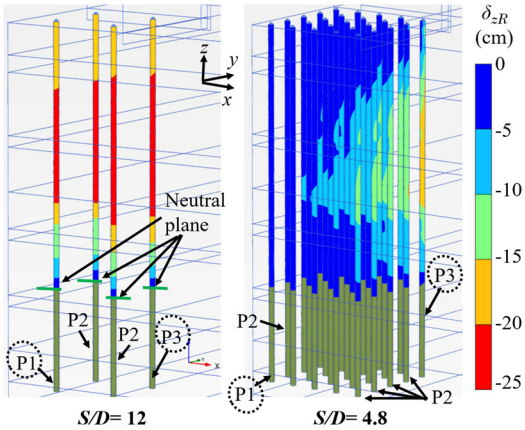

Figure 14. Vertical relative displacement fields, piles after 15 years.

5.5 *Pile axial load*

Figure 15 shows the axial load (*Q*) on P1 interior and P3 corner piles, which are highlighted in Figure 14. The short-term and long-term (before unloading each pile, replace the crushed cells and apply the preload) results are shown. An increase of the axial load on pile heads is evident. This is due to an increase in the pile apparent penetration. An increase in axial load due to negative skin friction is also observed. Axial loads in *S/D*=12 group are higher than those of the *S/D*=4.8 group for both piles. The P3 corner pile presents a higher axial load than the P1 interior pile for both groups. However, the difference is smaller in *S/D*=12 group than in the *S/D*=4.8 group.

5.6 *Slab vertical displacement*

Figure 16 shows the slab and wall deformation configurations for *S/D* = 4.8 and 12 groups at short-term and 15-year analysis stages. The deformed meshes are amplified 400 times the natural scale. In both groups, for the short-term analysis, the greatest vertical slab displacement is observed toward the

center due to the soil-structure interaction effects of the control piles (Domínguez-Alfaro, 2024). In the long-term, the *S/D*= 12 group presents a uniform slab displacement, whereas *S/D* = 4.8 group exhibits the lowest displacement at the center.

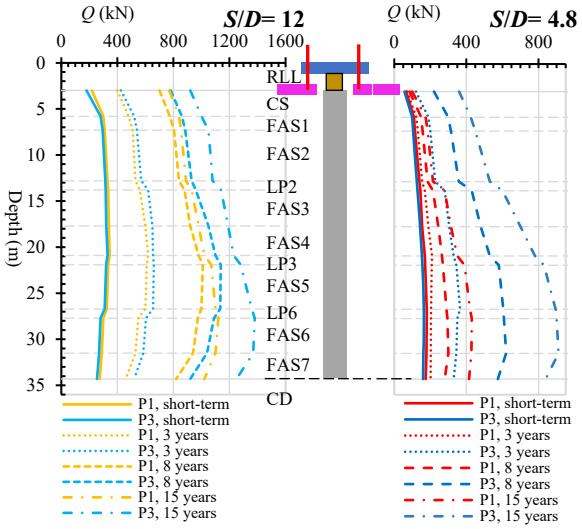

Figure 15. Axial load on the P1 (interior) and the P3 (corner) piles.

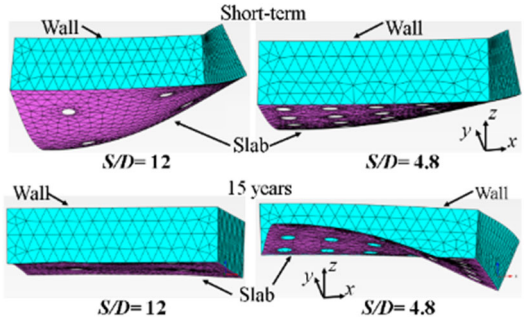

Figure 16. Deformed configurations of slab and walls.

5.7 *Discussion*

The above results reveal clear differences between the control pile groups. Therefore, it is confirmed that the number of control piles influences significantly the static long-term behavior of the foundation.

It is found that the development of negative skin friction influences the rest of the results (Figures 11 to 16). The development of negative skin friction depends on the interaction between the regional subsidence and the control piles. The greater the similarity of the magnitude of negative skin friction in the control piles, the more uniform the vertical displacement of the slab, the more uniform the apparent penetration of the piles, the more uniform the crushing of the deformable cells and the greater the need for maintenance. The greater the difference in negative skin friction between the P1 and the P3 piles, the greater the apparent protruding magnitude and the smaller the displacement of the slab in the center.

The behavior of the control pile group induced by negative skin friction depends on the number of piles (*S/D* ratio). Individual behavior occurs in groups with few control piles (high *S/D* ratio). Block behavior occurs in groups with many control piles (low *S/D* ratio).

6 CONCLUSIONS

The number of control piles was found to clearly influence the static long-term behavior of a new control pile foundation. The sequence of maintenance, the distribution of cell crushing, the magnitude of apparent protruding, the negative skin friction development, the slab vertical displacement, and the axial load on the piles all depend on the number of control piles.

A greater number of control piles will improve the safety of the foundation but will cause greater apparent protruding. Therefore, the design of foundations with control piles requires a delicate balance between the factors that influence static behavior and safety.

The parametric analysis presented in this paper is one of the five analyses performed by Domínguez-Alfaro (2024). The results of these five parametric analyses have provided a better understanding of the complex behavior of this special type of foundation, which has been widely used, but generally with empirical criteria. Analyzing this type of foundation with numerical models is recommended to consider such complex behavior. Currently, research continues to understand the seismic behavior of control piles and to develop constitutive models for deformable cells.

It is recommended to follow the methodologies proposed by Domínguez-Alfaro (2024) that allow: a) analyzing and calibrating the model used to represent numerically the regional subsidence, and b) analyzing and designing new foundations with control piles by means of numerical models.

7 REFERENCES

Auvinet, G. & Gutiérrez, E. 1990. *Instrumentación de un edificio en proceso de recimentación*. *Recimentaciones* (pp. 137-148). *Sociedad Mexicana de Mecánica de Suelos*. México.

Auvinet, G. Mendez, E. & Juárez, M. 2017. *El subsuelo de la Ciudad de México/The subsoil of Mexico City*, New edition, Vol. 3, Instituto de Ingeniería, UNAM, Mexico.

Auvinet, G. 2018. *Avances en la ingeniería de cimentaciones (1957-2017)*. Geotecnia, 249: 15-20. *Sociedad Mexicana de Ingeniería Geotécnica*. Mexico.

Carrillo, M. 1948. *Influence of artesian wells in the sinking of Mexico City*. Proceedings of the 2nd International Conference on Soil Mechanics and Foundation Engineering. Rotterdam.

Domínguez-Alfaro, R. 2024. *Evaluación numérica del comportamiento en grupo de pilotes de control*. National Autonomous University of Mexico. Master thesis. Mexico.

Domínguez-Alfaro, R., Auvinet, G., López-Acosta, N., Paniagua, W., Rivera, R., Pérez, M., Juárez, M. & Rodríguez, R. 2026. *Calibration of numerical model of regional subsidence for a site in Mexico City*. Proceedings of the 21st International Conference on Soil Mechanics and Foundation Engineering. Vienna.

Domínguez-Alfaro, R., Auvinet, G. & López-Acosta. 2026. *Numerical modelling of a box-type foundation with control piles, pile number effect.* Proceedings of the 8th International Young Geotechnical Engineering Conference. Graz.

González, M. 1948. *Level control in buildings by means of adjustable piling*. Proceedings of the 2nd International Conference on Soil Mechanics and Foundation Engineering. Rotterdam.

González, M. 1960. *Setting vertical two buildings: a meter in the most unfavorable case*. Proceedings of the 1st Panamerican Conference on Soil Mechanics and Foundation Engineering. Vol. 1. Mexico.

López-Acosta & Martinez, N. 2021. *Pilotes de control. Funcionamiento, diseño y aplicación*. (SID 710). II-UNAM.

Marsal, R., 1969. *Desarrollo de un lago por consolidación de arcillas blandas, inducida con bombeo. Nabor Carrillo: El hundimiento de la Ciudad de México*. 7th International Congress on Soil Mechanics and Foundation Engineering. Mexico.

PICOSA. 2014. *Ecuaciones para el diseño de capacidad de carga de González-Flores*. Report provided by *Pilotes de Control*, S.A. de C.V. to the Institute of Engineering. UNAM.

Reséndiz, D. & Auvinet, G. 1973. *Analysis of pile foundations in consolidating soils*. Proceedings of 8th International Conference on Soil Mechanics and Foundation Engineering. Moscow.

Tamez, E. 1990. *Criterios para el diseño sísmico de cimentación sobre pilotes de control*. Recimentaciones (pp. 5-18). *Sociedad Mexicana de Mecánica de Suelos.* México.

Zeevaert, E. 1983. *Foundation engineering for subsoil difficult conditions*. Van Nostrand Reinhold Company.